Atmospheric
Chemistry
and Physics
Discussions

The impact of aged wildfire smoke on atmospheric composition and ozone in the Colorado Front Range in summer 2015

Jakob Lindaas[1], Delphine K. Farmer[2], Ilana B. Pollack[1,2], Andrew Abeleira[2], Frank Flocke[3], Rob Roscioli[4], Scott Herndon[4], and Emily V. Fischer[1]

[1] Colorado State University, Department of Atmospheric Science, Fort Collins, CO, USA
[2] Colorado State University, Department of Chemistry, Fort Collins, CO, USA
[3] National Center for Atmospheric Research, Boulder, CO, USA
[4] Aerodyne Research Inc., Billerica, MA, USA

Correspondence to: Jakob Lindaas (jlindaas@rams.colostate.edu) or Emily V. Fischer (evf@rams.colostate.edu)

Abstract. The relative importance of wildfire smoke for air quality over the western U.S. is expected to increase as the climate warms and anthropogenic emissions decline. We report on *in situ* measurements of ozone (O_3), a suite of volatile organic compounds (VOCs), and reactive oxidized nitrogen species collected during summer 2015 at the Boulder Atmospheric Observatory (BAO) in Erie, CO. Aged wildfire smoke impacted BAO during two distinct time periods during summer 2015: 6 – 10 July and 16 – 30 August. The smoke was transported from the Pacific Northwest and Canada across much of the continental U.S. Carbon monoxide and particulate matter increased during the smoke-impacted periods, along with peroxyacyl nitrates and several VOCs that have atmospheric lifetimes longer than the transport timescale of the smoke. During the August smoke-impacted period, nitrogen dioxide was also elevated during the morning and evening compared to the smoke-free periods. There were six days during our study period where the maximum 8-hour average O_3 at BAO was greater than 65 ppbv, and two of these days were smoke-impacted. We examined the relationship between O_3 and temperature at BAO and found that for a given temperature, O_3 mixing ratios were greater (~10 ppbv) during the smoke-impacted periods. Enhancements in O_3 during the August smoke-impacted period were also observed at two long-term monitoring sites in Colorado: Rocky Mountain National Park and the Arapahoe National Wildlife Refuge near Walden, CO. Our data provide a new case study of how aged wildfire smoke can influence atmospheric composition at an urban site, and how smoke can contribute to increased O_3 abundances across an urban-rural gradient.

Keywords. wildfire smoke, air quality, ozone, *in situ* observations, biomass burning

1 Introduction

Over the past 30 years, wildfires in the western U.S. have increased in both frequency and intensity, and this trend will likely continue under future climate change (Westerling, 2016). Wildfire smoke can be transported over thousands of kilometers,

Atmospheric
Chemistry
and Physics
Discussions

Open Access

EGU

31 and exposure to wildfire smoke has significant impacts on human health (Künzli et al., 2006; Rappold et al., 2011; Elliott et

32 al., 2013). While U.S. emissions of most major air pollutants are declining (Pinder et al., 2008), increasing fire activity

33 suggests that wildfires may have a greater relative impact on U.S. air quality in the future (Val Martin et al., 2015).

34

35 Ozone (O_3) is formed when hydrocarbons are oxidized in the presence of nitrogen oxides ($NO_x = NO + NO_2$) and sunlight

36 (Sillman, 1999). Wildfires emit many trace gas species that contribute to tropospheric O_3 production. Along with carbon

37 monoxide (CO), methane (CH_4), and carbon dioxide (CO_2), hundreds of different non-methane volatile organic compounds

38 (NMVOCs) with lifetimes ranging from minutes to months (Atkinson and Arey, 2003) are emitted during biomass burning

39 (Akagi et al., 2011; Gilman et al., 2015). Due to relatively large emissions of CO_2, CO, CH_4 and NO_x, the contribution of

40 VOCs to the total emissions from fires on a molar basis is small (<1%). However, VOCs dominate the OH reactivity in

41 smoke plumes (Gilman et al., 2015). Recent observations of the evolution of VOCs within aging smoke plumes indicate that

42 OH can be elevated in young biomass burning plumes (Hobbs et al., 2003; Yokelson et al., 2009; Akagi et al., 2012; Liu et

43 al., 2016) in part due to the photolysis of oxygenated VOCs (Mason et al., 2001), which make a large contribution to the

44 total emitted VOC mass (Stockwell et al., 2015). Elevated OH may reduce the lifetime of emitted VOCs and increase

45 oxidation rates and potential O_3 production.

46

47 Fires are also a major source of oxidized nitrogen; emissions from biomass and biofuel burning represent approximately

48 15% of total global NO_x emissions (Jaegle et al., 2005). However, there are major uncertainties in NO_x emission estimates

49 from biomass burning, particularly at a regional scale (Schreier et al., 2015). NO_x emissions depend on the nitrogen content

50 of the fuel (Lacaux et al., 1996; Giordano et al., 2016) as well as the combustion efficiency (Goode et al., 2000; McMeeking

51 et al., 2009; Yokelson et al., 2009). Emitted NO_x is quickly lost in the plume, either by conversion to HNO_3 (Mason et al.,

52 2001) or via PAN formation (Alvarado et al., 2010; Yates et al., 2016). HNO_3 is not often observed in plumes because it

53 either rapidly forms ammonium nitrate or is efficiently scavenged by other aerosols (Tabazadeh et al., 1998; Trentmann et

54 al., 2005).

55

56 There are multiple lines of observational evidence indicating that wildfires in the western U.S. increase the abundance of

57 ground level O_3. Background O_3 mixing ratios across the western U.S. are positively correlated with wildfire burned area

58 (Jaffe et al., 2008), and daily episodic enhancements in O_3 at ground sites can be > 10 ppbv (Lu et al., 2016). There are well-

59 documented case studies of within plume O_3 production (Jaffe and Wigder, 2012) and time periods where smoke contributed

60 to exceedances of the U.S. EPA National Ambient Air Quality Standard (NAAQS) for O_3 (Morris et al., 2006; Pfister et al.,

61 2008). Brey and Fischer (2016) investigated the impacts of smoke on O_3 abundances across the U.S. via an analysis of

62 routine *in situ* measurements and NOAA satellite products. They found that the presence of smoke is correlated with higher

63 O_3 mixing ratios in many areas of the U.S., and that this correlation is not driven by temperature. Regions with the largest

64 smoke-induced O_3 enhancements (*e.g.* the southeast and Gulf coast) can be located substantially downwind of the wildfires

65 producing the most smoke.

66

67 Despite several recent studies showing that smoke contributes to elevated O_3, there have been relatively few detailed studies

68 of wildfire smoke mixing with anthropogenic air masses near the surface. Singh et al. (2012) used aircraft measurements

69 from summer 2008 over California to document significant O_3 enhancements in nitrogen-rich urban air masses mixed with

70 smoke plumes. Accompanying air quality simulations were not successful in capturing the mechanisms responsible for these

71 enhancements. In general, measurements of O_3 precursors are hard to make routinely. Instrumentation and calibration

72 methods tend to be time and labor intensive, and thus unpredictable wildfire smoke plumes and their effects on surface O_3

73 are sparsely sampled.

74

75 Here we present a case study of aged wildfire smoke mixed with anthropogenic pollution in the Colorado Front Range and

76 show its impact on atmospheric composition and O_3. This region violates the NAAQS for O_3, and has been the focus of

77 several recent studies (*e.g.* McDuffie et al., 2016; Abeleira et al., 2017). First we describe the research location and

78 measurements. Next, we identify the smoke-impacted time periods and show the origin, approximate age, and wide

79 horizontal extent of the smoke plumes. We characterize significant changes in atmospheric composition with respect to the

80 two major classes of O_3 precursors, VOCs and oxidized reactive nitrogen (NO_y). Finally, we present the impact of smoke on

81 O_3 abundances during this period and discuss the underlying causes of this impact.

82 **2 Measurements and Research Site**

83 During summer 2015, we made measurements of a suite of trace gases at the Boulder Atmospheric Observatory (BAO),

84 located north of Denver, CO, in the middle of the rapidly developing northern Colorado Front Range [40.05˚N, 105.01˚W,

85 1584m ASL]. BAO has a history of atmospheric trace gas and meteorological measurements stretching back nearly four

86 decades (Kelly et al., 1979; Gilman et al., 2013). Our research campaign from 1 July – 7 September 2015 measured a suite

87 of O_3 precursor species as well as several NO_x oxidation products and greenhouse gases. The intended goal of the field

88 campaign was to improve our understanding of the complex O_3 photochemistry in the Colorado Front Range and the

89 contributions of oil and natural gas activities as well as other anthropogenic emissions to O_3 production. All measurements

90 were made by instruments housed in two trailers located at the base of the BAO tower. Here we briefly describe the

91 measurements used in this paper. Data are available at https://esrl.noaa.gov/csd/groups/csd7/measurements/2015songnex/.

92

93 We measured CO and CH_4 at ~3 second time resolution with a commercial cavity ring-down spectrometer (Picarro, model

94 G2401) (Crosson, 2008). The inlet was located 6 m above ground level (a.g.l.), and a 1 μm PTFE filter membrane (Savillex)

95 at the inlet was changed weekly. Laboratory instrument calibrations were performed pre- and post-campaign using three

96 NOAA standard reference gases (http://www.esrl.noaa.gov/gmd/ccl/refgas.htmls; CA06969, CB10166, and CA08244). Field

97 calibration was performed every 3 hours using high, low and middle reference gas mixtures (Scott Marin Cylinder IDs

98 CB10808, CB10897, CB10881). Mixing ratios were calculated using the WMO-CH4-X2004 and WMO-CO-X2014 scales.

99 The uncertainty associated with the CH_4 and CO data is estimated to be 6% and 12% respectively, and it was estimated as

100 the quadrature sum of measurement precision, calibration uncertainty and uncertainty in the water vapor correction.

101

102 A custom 4-channel cryogen free gas chromatography (GC) system (Sive et al., 2005) was used to measure selected non-

103 methane hydrocarbons (NMHCs), $C_1 - C_2$ halocarbons, alkyl nitrates (ANs), and oxygenated volatile organic compounds

104 (OVOCs) at sub-hourly time resolution. The inlet was located at 6 m a.g.l. with a 1 μm teflon filter. A calibrated whole air

105 mixture was sampled in the field after every ten ambient samples to monitor sensitivity changes and measurement precision.

106 A full description of this instrument is provided in (Abeleira et al., 2017).

107

108 Ozone data at BAO for this time period were provided by the NOAA Global Monitoring Division surface ozone network

109 (McClure-Begley et al., 2014; data available at aftp.cmdl.noaa.gov/data/ozwv/SurfaceOzone/BAO/). Ozone was measured

110 via UV-absorption using a commercial analyzer (Thermo-Scientific Inc., model 49), which is calibrated to the NIST standard

111 over the range 0 – 200 ppbv and routinely challenged at the site. The inlet height was 6m a.g.l. on the BAO tower, located

112 about 50 feet from the two trailers, and measurements were reported at a 1 minute averaging interval with an estimated error

113 of 1%.

114

115 Nitrogen oxides ($NO_x≡NO+NO_2$) and total reactive nitrogen (NO_y) were measured via $NO-O_3$ chemiluminescence detection

116 (Kley and McFarland, 1980) using a commercial analyzer (Teledyne, model 200EU). Two commercial converters, a 395 nm

117 -LED converter (Air Quality Designs, Inc., model BLC) for chemically-selective photolysis of NO_2 to NO and a

118 molybdenum in stainless steel converter (Thermo Scientific Inc.) heated to 320 ºC for reduction of NO_y to NO, were

119 positioned as close to the inlet tip as possible (<10 cm). A 7 μm stainless steel particulate filter was affixed to the upstream

120 end of the molybdenum converter; otherwise no other filters were used. The analyzer switched between sampling from the

121 LED (NO_x) converter and the molybdenum (NO_y) converter every 10 seconds, and the LEDs were turned on (to measure

122 $NO+NO_2$) and off (to measure NO only) every minute. NO_2 was determined by subtraction of measured NO from measured

123 $NO+NO_2$ divided by the efficiency of the LED converter. All three species are reported on a consistent two-minute average

124 timescale. The detector was calibrated daily by standard addition of a known concentration of NO, NIST-traceable (Scott-

125 Marrin Cylinder ID CB098J6), to synthetic ultrapure air. Both converters were calibrated with a known concentration of NO_2

126 generated via gas phase titration of the NO standard. The NO_y channel was further challenged with a known mixing ratio of

127 nitric acid (HNO_3) generated using a permeation tube (Kintech, 30.5 ± 0.8 ng/min at 40 ºC), which was used to confirm

128 >90% conversion efficiency of HNO_3 by the molybdenum converter. Uncertainties of ±5% for NO, ±7% for NO_2, and ±20%

129   for NO_y are determined from a quadrature sum of the individual uncertainties associated with the detector, converters, and

130   calibration mixtures; an LOD of 0.4 ppbv for all species is dictated by the specifications of the commercial detector.

131

132   Peroxyacyl nitrates (PANs) were measured using the National Center for Atmospheric Research gas chromatograph with an

133   electron capture detector (NCAR GC-ECD) (Flocke et al., 2005). The instrument configuration was the same as was used

134   during the summer 2014 FRAPPE field campaign (Zaragoza, 2016). The NCAR GC-ECD analyzed a sample every five

135   minutes from a 6 m a.g.l. inlet with 1µm teflon filter. A continuous-flow acetone photolysis cell generated a known quantity

136   of PAN used to calibrate the system at 4-hour intervals.

137

138   An Aerodyne dual quantum cascade laser spectrometer was used to measure HNO_3 (McManus et al., 2011). The instrument

139   employed a prototype 400 m absorption cell for increased sensitivity during the first month of the campaign, after which it

140   was replaced by a 157 m absorption cell. An active passivation inlet (Roscioli et al., 2016) was used to improve the time

141   response of the measurement to ~0.75 s. This technique utilized a continuous injection of 10-100 ppb of a passivating agent

142   vapor, nonafluorobutane sulfonic acid, into the inlet tip. The inlet tip was made of extruded perfluoroalkoxy Teflon (PFA),

143   followed by a heated, fused silica inertial separator to remove particles larger than 300 nm from the sample stream. The inlet

144   was located 8 m a.g.l. with a 18 m heated sampling line (PFA, 1/2" diameter OD) to the instrument. The system was

145   calibrated every hour by using a permeation tube that was quantified immediately prior to the measurement period.

146   **3 Smoke Events**

147   We observed two distinct smoke-impacted periods at BAO, identified by large enhancements in CO and fine aerosol ($PM_{2.5}$).

148   Figure 1 presents CO observations from BAO and fine particulate matter ($PM_{2.5}$) observations from the Colorado

149   Department of Public Health and Environment (CDPHE) CAMP air quality monitoring site, located in downtown Denver,

150   approximately 35km south of BAO. $PM_{2.5}$ was similarly elevated during the smoke-impacted periods at CDPHE monitoring

151   sites across the Colorado Front Range (not shown). For our analysis, we defined a July smoke-impacted period and an

152   August smoke-impacted period. The July smoke-impacted period lasted for 4 days from 00 MDT 6 July 2015 to 00 MDT 10

153   July 2015. The August smoke-impacted period was significantly longer (~14 days). For the subsequent analysis, we

154   combined three distinct waves of smoke-impact in this 14 day period into one August smoke-impacted period: 00 MDT 16

155   August 2015 – 18 MDT 21 August 2015, 12 MDT 22 August 2015 – 18 MDT 27 August 2015, and 14 MDT 28 August

156   2015 – 09 MDT 30 August 2015. We omitted the brief periods between these times from the analysis due to uncertainty on

157   the influence of smoke during them. All other valid measurements were considered part of the smoke-free data.

158

159   Figure 2 presents the extent of the presence of smoke in the atmospheric column during representative smoke-impacted days,

160   7 July and 21 August 2015. The NOAA Hazard Mapping System smoke polygons (grey shading) show that the smoke

161 events observed at BAO were large regional events. The HMS smoke product is produced using primarily visible satellite

162 imagery (Rolph et al., 2009). The extent of smoke plumes within the HMS dataset represents a conservative estimate, and no

163 information is provided on the vertical extent or vertical placement of the plumes. The red triangles represent MODIS active

164 fire locations for the previous day (Giglio et al., 2003; Giglio et al., 2006). The thin black lines are NOAA Air Resources

165 Laboratory (ARL) Hybrid Single Particle Lagrangian Integrated Trajectory (HYSPLIT) 120 hour backward trajectories

166 initialized each hour of the day from BAO at 1000m above ground level (Stein et al., 2015). Trajectories were run using the

167 EDAS (Eta Data Assimilation System) 40 km x 40 km horizontal resolution reanalysis product (Kalnay et al., 1996). Figure

168 2 shows the smoke that impacted BAO during both periods was transported from large fire complexes in the Pacific

169 Northwest and Canada, with approximate transport timescales on the order of two to three days. Creamean et al. (2016)

170 provide a more detailed description of smoke transport and the sources of the aerosols associated with the August smoke-

171 impacted period.

172 **4 Observed Changes in Ozone and its Precursors**

173 **4.1 CO, CH$_4$, and VOC Abundances**

174 We quantified CO, CH$_4$, and 40+ VOC species including C$_2$-C$_{10}$ non-methane hydrocarbons (NMHCs), C$_1$-C$_2$ halocarbons,

175 and several oxygenated species (methyl ethyl ketone, acetone, and acetaldehyde) at BAO. The focus of the BAO field

176 intensive was to study the photochemistry of local emissions from oil and gas development (*e.g.* Gilman et al., 2013;

177 Swarthout et al., 2013; Thompson et al., 2014; Abeleira et al., in review), and we did not quantify species with known large

178 biomass burning emission ratios (*e.g.* hydrogen cyanide, acetonitrile, most oxygenated organic species). In addition, early

179 campaign issues with the online multichannel gas chromatography system compromised the data for the July smoke period

180 and thus we restrict our comparison of VOCs in smoke-free versus smoke-impacted periods to a comparison between 16 –

181 30 August, the *August smoke-impacted period*, and 24 July – 16 August, the *smoke-free period*. The brief smoke-free times

182 during 16 – 30 August (denoted by white between the red shading in Figure 1) were not included in either period since it is

183 difficult to determine whether they were smoke-impacted. GC measurements were made approximately every 50 minutes

184 and we compared 251 measurements of VOCs during the August smoke-period to 583 measurements during the smoke-free

185 period.

186

187 In this section, we describe significant changes in VOC abundances and notable exceptions. The HYSPLIT trajectories

188 (Figure 2) suggest that the age of the smoke impacting the Front Range during the August smoke-period was 2-3 days. We

189 observed enhancements in the abundances of CO, CH$_4$, and VOCs with lifetimes longer than the transport time of the smoke,

190 with the exception of some alkanes that have a large background concentration in the Front Range due to emissions from oil

191 and gas production. The alkenes we quantified (isoprene, ethene, and propene) were generally near the limit of detection

Atmospheric
Chemistry
and Physics
Discussions

192   during the August smoke-impacted period, although notably cis-2-butene abundances were not changed. Significant

193   differences were not observed in the four oxygenated VOCs quantified between smoke-impacted and smoke-free periods.

194

195   Mean CO mixing ratios were significantly enhanced by 86 ppbv, or 65%, during the August smoke-impacted period (Figure

196   1). This enhancement was present across the diurnal cycle (Figure 3) and a greater range of CO mixing ratios (96 – 402 ppbv

197   versus 70 – 291 ppbv) were measured during the August smoke-impacted period compared to the smoke-free period.

198   Average enhancements of CH_4 were a much smaller percentage of (~3% or 67 ppbv), but comparable in magnitude to, the

199   CO mixing ratio enhancement. Methane has a relatively high background at BAO due to large emissions of CH_4 in nearby

200   Weld County from livestock production and oil and gas development (Pétron et al., 2014; Townsend-Small et al., 2016).

201   Taken together, the larger background of CH_4 and the large local sources of CH_4 in the Front Range served to mute the

202   impact of the August smoke on overall CH_4 abundances. The diurnal cycle of CH_4 did not change during the smoke-

203   impacted period as compared to the smoke-free period and we observed a similar range of mixing ratios (~1,840 – 3,360

204   ppbv) in the both smoke-free and smoke-impacted periods. We note several large spikes on the order of minutes during the

205   smoke-impacted period, but we do not believe that these are related to the presence of smoke because they were not

206   correlated with similar excursions in CO and PANs, and exhibited strong correlations with propane and other tracers of oil

207   and gas and other anthropogenic activity.

208

209   Similar to CO, ethane has an atmospheric lifetime on the order of a month during summertime at mid-latitudes (Rudolph and

210   Ehhalt, 1981) and is emitted by wildfires (Akagi et al., 2011). However, average ethane mixing ratios were not higher during

211   the August smoke-impacted period compared to the smoke-free period. One potential reason for this may be the large local

212   sources of alkanes from oil and natural gas activities within the Denver-Julesberg Basin which contribute to relatively high

213   local mixing ratios of these species (Gilman et al., 2013; Swarthout et al., 2013; Thompson et al., 2014; Abeleira et al.,

214   2017). The range of ethane mixing ratios observed at BAO was also not different between smoke-free (0.3 - 337 ppbv) and

215   smoke-impacted periods (1 – 362 ppbv), but the amplitude of the median diurnal cycle was dampened during the August

216   smoke-impacted period (not shown). Median morning ethane mixing ratios were ~10 – 20 ppbv less during smoke-impacted

217   than smoke-free periods, while afternoon and evening median mixing ratios were ~5 – 10 ppbv larger. Most of the $C_3 – C_9$

218   alkanes we quantified showed similarly dampened amplitudes in their median smoke-period diurnal cycles. A consistently

219   lower planetary boundary layer (PBL) height during the day and a consistently higher boundary layer at night is one

220   potential explanation for these observations; however an estimate of the PBL height in the grid box surrounding BAO from

221   the North American Regional Reanalysis product (Mesinger et al., 2006) did not show any significant changes in PBL height

222   between the smoke-impacted and smoke-free periods. Likewise estimated PBL heights following methods from Coniglio et

223   al. (2013) and using atmospheric soundings at 0Z and 12Z in Denver (http://mesonet.agron.iastate.edu/archive/raob/) did not

224   show any differences between smoke-impacted and smoke-free periods (Figures S1 and S2). Figure 3 shows there were two

225   exceptions to the general alkane pattern noted above: 2-methylhexane showed a significant decrease in average abundances

7

Atmospheric
Chemistry
and Physics
Discussions

226   (-39 pptv or -45%) and 3-methylhexane showed a significant increase (63 pptv or 75%) during the smoke-impacted period,

227   despite both having similar smoke-free abundances and similar rate constants for reaction with OH radicals ($\sim 7 \times 10^{12}$ cm^3

228   molec^{-1} s^{-1}).

229

230   The atmospheric lifetimes of the four alkenes we quantified (isoprene, propene, ethene, and cis-2-butene) range from tens of

231   minutes to hours. Isoprene, propene, and ethene showed significant decreases in their average abundance: -64% (-143 pptv),

232   -77% (-39 pptv), and -81% (-206 pptv) respectively. The shape of the diurnal cycles did not change (not shown), though

233   propene and ethene were near their respective limits of detection for the majority of each day during the smoke-impacted

234   period. These alkenes were among the most reactive species quantified, and one potential explanation for the reduced

235   abundance of these species during the smoke-impacted period is enhanced oxidation capacity linked to the presence of

236   smoke. However, we do not observe decreased abundances of cis-2-butene, which has a comparable OH-reactivity to

237   propene and lower average abundance. An alternative hypothesis for the reductions in the other three alkene species may be

238   reductions in local biogenic emissions during the smoke-impacted period either due to lower air temperatures or due to a

239   reduction in photosynthetic active radiation (PAR) at the surface during the August smoke-impacted period. Isoprene is

240   emitted by broad leaf vegetation, and emission rates are highly light and temperature sensitive (Guenther et al., 2006).

241   However, while we did observe lower average daytime temperatures at BAO during the August smoke-impacted period

242   compared to the rest of the dataset (-2.3˚C), the majority of Front Range emissions of propene and ethene are likely from

243   anthropogenic sources. Thus this hypothesis could possibly help explain reduction in isoprene but not likely explain

244   reductions in ethene and propene. Shifts in local transport could also help explain differences but we did not observe any

245   consistent shifts in wind direction or changes in wind speed that would indicate consistently different local transport during

246   the August smoke-impacted period.

247

248   The only alkyne measured was ethyne. Ethyne is emitted by wildfires (Akagi et al., 2011) and has a lifetime of ~1 month

249   during summer. We observed a significant increase in the abundance of ethyne during the August smoke-impacted period.

250   These enhancements were small in absolute mixing ratio (0.163 ppbv), but represented a large percentage increase (67%)

251   and were consistently present throughout the day.

252

253   It is well known that wildfires produce carcinogenic aromatic hydrocarbons including benzene (Fent et al., 2014). During the

254   smoke-impacted periods, we observed significantly enhanced benzene throughout the day with an average increase of 0.117

255   ppbv and a percentage increase of 67%. These enhancements followed the pattern of CO and ethyne; there were consistent

256   increases throughout the day and the diurnal cycle retained its shape. Wildfires also produce toluene (Fent et al., 2014);

257   however, it has a substantially shorter lifetime (< 2 days) than benzene (~12 days). Toluene showed no significant changes in

258   its mean mixing ratio, diurnal cycle, or range of values measured at BAO during the smoke-impacted periods. The other

259   aromatic hydrocarbons we quantified (o-xylene and ethyl-benzene) also did not change significantly.

260

261   As mentioned in Section 1, oxygenated VOCs are emitted by wildfires and make a large contribution to the total emitted

262   VOC mass in wildfire smoke (Stockwell et al., 2015). Additionally they are produced as oxidation intermediates (Atkinson

263   and Arey, 2003). Acetaldehyde, acetone, and methyl ethyl ketone (MEK) showed no consistent changes in their abundances,

264   diurnal cycles, or range during the smoke-impacted period compared to the smoke-free period. Small increases in average

265   acetone (~350 pptv) and MEK (~150 pptv) mixing ratios during late afternoon and evening hours were not statistically

266   significant.

267

268   Given the diversity of emission sources across the northern Colorado Front Range, previous studies of atmospheric

269   composition at BAO have noted a strong dependence of VOC composition on wind direction (Pétron et al., 2012; Gilman et

270   al., 2013). Recent housing development and oil and gas production surrounding the BAO site have made analyses based on

271   wind direction more challenging in recent years (McDuffie et al., 2016). Importantly for our analysis, we found that the

272   statistically significant changes in all species during the smoke-impacted periods occurred across all wind directions. Figure

273   4 shows this for two example species: benzene and NO_2. We also did not find statistically significant changes in wind

274   direction or wind speed patterns between smoke-free and smoke-impacted periods. Thus we attribute the changes in

275   atmospheric composition during the August smoke-impacted period to the presence of smoke.

4.2 Reactive Oxidized Nitrogen (NO_y) Species

277   Peroxyacyl nitrates and HNO_3 were successfully measured from 10 July – 7 September and alkyl nitrates were measured

278   from 24 July – 30 August. Thus we report significant changes in these species for the August smoke-impacted period only.

279   We observed significant enhancements in both peroxyacetyl nitrate (PAN) and peroxypropionyl nitrate (PPN) during the

280   August smoke-impacted period. PAN and PPN abundances were consistently elevated across the day by an average of 183

281   and 22 pptv respectively, corresponding to a ~100% change for both species. The peak of each diurnal cycle was shifted later

282   in the day by about 3-4 hours for the smoke-impacted period. This cannot be accounted for merely by the shift in the timing

283   of solar noon given that the total decrease in daylight between 10 July and 30 August is ~2 hours. The ratio of PPN to PAN

284   during the August smoke-impacted period exhibited a significant decrease from the smoke-free period ratio (0.14 ± 0.012

285   versus 0.17 ± 0.006; calculated as the slope of a reduced major axis linear regression on the hourly data from 12PM – 5PM

286   MDT Figure S3). The direction of change in the ratio is consistent with observations of PPN/PAN ratios in Asian urban and

287   aged biomass burning plumes off the coast of California (Roberts et al., 2004). The $C_1 – C_2$ alkyl nitrates measured at BAO

288   exhibited similar behaviors; methyl nitrate and ethyl nitrate saw average enhancements during the August smoke period of

289   1.2 and 0.77 pptv, 41% and 31% respectively, though the average mixing ratios of these species are smaller by an order of

290   magnitude compared to other alkyl nitrates quantified. Propyl-, pentyl-, and butyl-nitrate did not display significant changes

291   in their average mixing ratio, though we observed a similar shift in the peak of their diurnal cycles of 2-4 hours. We did not

292   observe significant changes in the abundances of HNO_3. There were no changes to the diurnal cycle or the range of mixing

293   ratios observed.

294

295   NO and NO_2 measurements were made during the entire campaign, 1 July – 7 September 2015, so both the July and August

296   smoke-impacted periods were analyzed with respect to potential changes in NO_x. NO was present in the same abundances

297   between the two periods and showed the same diurnal cycle during the August smoke-impacted period as compared to the

298   smoke-free period (Figure 5). During the July smoke-impacted period the morning buildup of NO was slower than the

299   smoke-free period, though the mixing ratios were within the range of smoke-free values and there were fewer days in the

300   July period compared to the August smoke-impacted period.

301

302   Figure 5 shows that NO_2 abundances exhibited more significant changes. During the July smoke-impacted period, NO_2 was

303   within the range of smoke-free measurements but the diurnal cycle was shifted later in the day and the average decrease in

304   mixing ratios of NO_2 in the afternoon was not as strong as during the smoke-free periods. In contrast NO_2 during the August

305   smoke-impacted period followed the same diurnal cycle but had pronounced significant increases in average mixing ratios

306   during the morning and evening hours of ~8 ppbv (17%) following sunrise and 3 ppbv (60%) following sunset. These

307   enhanced peak abundances appeared during multiple days during the August smoke-impacted period. We did not find

308   evidence that these enhancements were due to traffic patterns. The concurrently observed PAN abundances can only account

309   for at most 1 ppbv of additional NO_2, but there could have been significantly higher PAN abundances in the smoke plume

310   prior to reaching BAO and PAN dissociation is one hypothesis for the enhanced abundances. We do not have measurements

311   of other reactive nitrogen species (e.g. HONO, $ClNO_2$, NO_3, and N_2O_5) to test potential other hypotheses of a different

312   chemical mechanism to explain the observed NO_2 enhancements.

313   **4.3 Ozone**

314   As discussed in the introduction, wildfire smoke has been found to produce O_3 within plumes and to be correlated with

315   enhanced surface O_3 in areas to which it is advected. The total amount of O_3 at a location is a complex combination of the

316   relative abundances of VOCs and NO_x, meteorological conditions supporting local O_3 production, and the amount of O_3

317   present in the air mass before local production. In this section we describe the significant increases in O_3 during both smoke-

318   impacted periods, show that these enhancements were most likely not due to changes in meteorological conditions, and

319   discuss evidence pointing to whether these changes may be due to enhanced local production or transport of O_3 produced

320   within the smoke plume.

321

322   Figure 5d shows that there were significant increases in O_3 mixing ratios during nighttime and midday during the August

323   smoke-impacted period compared to the average smoke-free diurnal cycle. The mean O_3 mixing ratio across all hours of the

324   day was 6 ppbv (14%) larger during the August smoke-impacted period than the smoke-free period (Figure 6), significant at

325   the 99% confidence level based on a two-sample difference of means t-test. There were no significant changes in the average

326   O_3 mixing ratios during the July smoke-impacted period (Figure 5a). The average mixing ratio of O_3 during the July smoke-

327   impacted period was not greater than absolute average during the smoke-free period (Figure 5a). However, as discussed in

328   Section 2, this period in particular was much colder on average than the smoke-free period.

329

330   O_3 mixing ratios generally increase with temperature, and this relationship has been attributed to 1) warm and often stagnant

331   anti-cyclonic atmospheric conditions that are conducive to O_3 formation, 2) warmer air temperatures that reduce the lifetime

332   of PAN, releasing NO_2, and 3) lower relative humidity that reduces the speed of termination reactions to the O_3 production

333   cycle (Jacob et al., 1993; Camalier et al., 2007). Figure 6 presents hourly average O_3 and temperature at BAO and shows a

334   positive relationship between O_3 and temperature for both the smoke-free period in black and August smoke-impacted period

335   in red. The increase in O_3 mixing ratios during the August smoke-impacted period compared to the smoke-free period is

336   present across the entire range of comparable temperatures. Figure S4 shows the same result during the July smoke-period,

337   where for comparable temperatures the July smoke-period has higher O_3 than would be expected from the O_3-temperature

338   relationship during the smoke-free period. Across both smoke-impacted periods and for a given temperature, the magnitude

339   of the increase in average O_3 was 10 ± 2 ppbv. This was calculated as the mean difference between medians within each

340   temperature bin weighted by the total number of hourly measurements within each bin. The weighted standard deviation was

341   calculated in the same way. The magnitude of this difference is greater than the average difference in means between the

342   smoke-free O_3 mixing ratios and the August smoke-impacted period because there were several periods during the July and

343   August smoke-impacted period where air temperatures were colder (~ 5°C) than most observations during the smoke-free

344   period. Thus the lower O_3 mixing ratios associated with these smoke-impacted periods (*e.g.* ~ 20 - 40 ppbv) were not

345   included in the weighted difference in medians since there were not commensurate smoke-free O_3 measurements at those

346   same temperatures.

347

348   In addition to a positive relationship with surface temperature, elevated O_3 in the western U.S. has also been found to be

349   correlated with 500 hPa geopotential heights, 700 hPa temperatures, and wind speeds (Reddy and Pfister, 2016). We tested

350   the relationship between O_3 and these meteorological variables during our study period using observations from the 0Z and

351   12Z atmospheric soundings conducted in Denver (http://mesonet.agron.iastate.edu/archive/raob/). We did not find a

352   relationship between O_3 and daily 500 hPa geopotential heights or 700 hPa temperatures, nor were these meteorological

353   variables notably elevated during the August smoke-impacted period (Figures S5, S6, and S7). Additionally we did not find

354   a significant change in wind speed during the August smoke-impacted period. Thus we have no evidence that the enhanced

355   O_3 during the August smoke-impacted period was due to meteorological factors.

356

357   To determine if a change in synoptic scale transport in smoke-impacted versus smoke-free periods could have contributed to

358   different abundances, we performed a k-means cluster analysis on 72-hour HYSPLIT back trajectories. The trajectories were

Atmospheric
Chemistry
and Physics
Discussions

359   calculated using the methods described above, and initiated each hour at 2000 m a.g.l. from BAO. We chose to initialize the

360   trajectories at 2000 m a.g.l so that fewer trajectories intersect the ground in the Rocky Mountains. Trajectories are unlikely

361   to capture the complex circulations (*e.g.* potential Denver Cyclones or up/down slope winds) characteristic of summertime in

362   the Front Range, but they should capture synoptic scale air mass motions. The k-means analysis clustered each trajectory

363   into a predetermined number of clusters by minimizing the distance between each trajectory and its nearest neighbor; this

364   technique has been used to classify air mass history in air quality studies (Moody et al., 1998). We found 4 predominate

365   trajectory clusters during our study period: northwesterly flow, westerly flow, southwesterly flow, and local/indeterminate

366   flow (Figure S8). We then compared afternoon (12PM – 5PM MDT) hourly O_3 measurements separated by trajectory cluster

367   and binned by temperature between the smoke-free period and the August smoke-impacted period. Most hours during the

368   August smoke-impacted period were associated with northwesterly flow and we found the same enhancement in O_3 for a

369   given temperature when comparing smoke-impacted observations to smoke-free observations assigned to this cluster as we

370   found for the complete dataset (Figures S9 and S10). Thus we conclude that potential changes in O_3 driven by synoptic scale

371   transport conditions cannot account for the observed O_3 enhancements during the August smoke-impacted period at BAO.

372

373   We calculated the maximum daily 8 hour average (MDA8) O_3 mixing ratios, following methodology from the U.S. EPA,

374   and found that out of 6 high O_3 days at BAO (defined as > 65 ppbv MDA8) during our study period, 2 occurred during the

375   August smoke-impacted period (Figure 7). As we stated above, elevated O_3 during the smoke period was not a result of

376   abnormal meteorological variables such as higher than normal temperatures, and thus these 2 high O_3 days are very likely

377   caused in part due to the presence of wildfire smoke. The lower portion of Figure 7 again shows that maximum daily

378   temperatures during the smoke-impacted periods were the same as or lower than maximum daily temperatures during the

379   smoke-free period.

380

381   To assess the spatial extent of the O_3 enhancements observed at BAO and to investigate the relative likelihood of O_3

382   enhancements due to transport within the smoke versus greater local production, we analyzed hourly O_3 measurements from

383   two nearby National Park Service (NPS) Air Resources Division (http://ard-request.air-resource.com/data.aspx)

384   measurement locations. The Rocky Mountain National Park long-term monitoring site (ROMO; 40.2778˚N, 105.5453˚W,

385   2743 meters A.S.L.) is located on the east side of the Continental Divide and co-located with the Interagency Monitoring of

386   Protected Visual Environments (IMPROVE) and EPA Clean Air Status and Trends Network (CASTNet) monitoring sites.

387   Front Range air masses frequently reach this site during summer afternoons (Benedict et al., 2013). The Arapahoe National

388   Wildlife Refuge long-term monitoring site (WALD; 40.8822˚N, 106.3061˚W, 2417 meters A.S.L.) near Walden, Colorado,

389   is a rural mountain valley site with very little influence from anthropogenic emissions. Figure 8 shows that the August

390   smoke-impacted period produced increases in O_3 mixing ratios across all three sites.

391   When comparing afternoon data for a given temperature, there are enhancements of 10 ± 2 ppbv, 12 ± 3 ppbv, and 4 ± 2

392   ppbv O_3 at BAO, ROMO and WALD respectively. O_3 enhancements across all three sites, across an approximate urban to

393   rural gradient, suggest that some amount of the O_3 enhancement observed at BAO during the August smoke-impacted period

394   is the result of O_3 production within the plume during transit. As for enhanced local production of O_3, we do not find any

395   significant differences in average calculated ozone production efficiency (OPE) between the smoke-impacted and smoke-

396   free periods (Figure S11) but the VOC composition changes suggest possible enhanced oxidation capacity during the August

397   smoke period. Fully addressing the question of whether the smoke enhanced local O_3 production in the polluted Front Range

398   requires the use of a chemical transport model, and is beyond the scope of this work.

5 Conclusions

400   Here we report a time series of detailed gas-phase ground measurements in the northern Colorado Front Range during

401   summer 2015. Clear anomalies in CO and $PM_{2.5}$ showed that aged wildfire smoke was present at ground-level during two

402   distinct periods (6 – 10 July and 16 – 30 August) for a total of nearly three out of the nine weeks sampled. This smoke from

403   wildfires in the Pacific Northwest and Canada impacted a large area across much of the central and western U.S., and was

404   several days old when it was sampled in Colorado. This wildfire smoke mixed with anthropogenic emissions in the Front

405   Range, resulting in significant changes in the abundances of O_3 and many of its precursor species. Our measurements are

406   unique because of 1) the length of time we sampled this smoke-impacted anthropogenic air mass, and 2) the detailed

407   composition information that was collected.

409   During the smoke-impacted periods we observed significantly increased abundances of CO, CH_4, and several VOCs with

410   OH oxidation lifetimes longer than the transport time of the smoke. We measured significant decreases in several of the most

411   reactive alkene species, indicating possible enhanced oxidation processes occurring locally. Mixing ratios of peroxyacyl

412   nitrates and some alkyl nitrates were enhanced and peak abundances were delayed by 3-4 hours, but there was no significant

413   change in HNO_3 mixing ratios or its diurnal cycle. During the longer August smoke-impacted period we observed significant

414   increases in NO_2 mixing ratios just after sunrise and sunset. We did not observe any consistent shifts in wind direction or

415   changes in wind speed that can explain the observed changes in composition, and the changes in abundances that we

416   observed for a given species were generally present across all directions and speeds.

418   We observed significantly enhanced O_3 abundances of about 10 ppbv for any given temperature during both smoke-impacted

419   periods. The enhancements during the August smoke-period led to very high surface O_3 levels; out of 6 high O_3 days at BAO

420   during our study period, 2 were during the August smoke-period and were impacted by wildfire smoke. These enhancements

421   were not due to higher temperatures, nor anomalous meteorological conditions. We found evidence of O_3 produced within

422   the smoke plume during transit, with potentially enhanced local production as well due to enhanced oxidation capacity.

Atmospheric
Chemistry
and Physics
Discussions

424 It is important to note that the presence of smoke does not always result in very high O_3 abundances. Many other factors

425 contribute to the overall level of surface O_3, and smoke can also be associated with decreased O_3 at times, such as during the

426 July smoke event described herein. Each smoke event has unique characteristics and thus it is important to study and

427 characterize more events such as these in the future.

428

429 Wildfire smoke during these time periods most likely impacted atmospheric composition and photochemistry across much of

430 the mountain west and great plains regions of the U.S. Given the BAO, Rocky Mountain and Walden research locations span

431 an urban-rural gradient as well as a large altitudinal gradient, it is likely that both rural and urban locations impacted by this

432 smoke could have experienced enhanced O_3 levels. Wildfires are increasing in both frequency and intensity throughout the

433 western U.S. due to climate change and thus wildfire smoke events such as this one will likely play an increasingly prevalent

434 role in degrading U.S. air quality.

435

436 **Author Contribution:** J. L. compiled and analysed the data, and wrote the manuscript. All authors participated in data

437 collection at BAO and contributed to the writing of or provided comments on the manuscript.

438

444 **References**

445 Abeleira, A., Pollack, I. B., Sive, B., Zhou, Y., Fischer, E. V., and Farmer, D. K.: Source Characterization of Volatile Organic Compounds
446   in the Colorado Northern Front Range Metropolitan Area during Spring and Summer 2015, Journal of Geophysical Research:
447   Atmospheres, 122, doi:10.1002/2016JD026227, 2017.
448 Akagi, S. K., Yokelson, R. J., Wiedinmyer, C., Alvarado, M. J., Reid, J. S., Karl, T., Crounse, J. D., and Wennberg, P. O.: Emission
449   factors for open and domestic biomass burning for use in atmospheric models, Atmos. Chem. Phys., 11, 4039-4072,
450   10.5194/acp-11-4039-2011, 2011.
451 Akagi, S. K., Craven, J. S., Taylor, J. W., McMeeking, G. R., Yokelson, R. J., Burling, I. R., Urbanski, S. P., Wold, C. E., Seinfeld, J. H.,
452   Coe, H., Alvarado, M. J., and Weise, D. R.: Evolution of trace gases and particles emitted by a chaparral fire in California,
453   Atmos. Chem. Phys., 12, 1397-1421, 10.5194/acp-12-1397-2012, 2012.
454 Alvarado, M. J., Logan, J. A., Mao, J., Apel, E., Riemer, D., Blake, D., Cohen, R. C., Min, K. E., Perring, A. E., Browne, E. C.,
455   Wooldridge, P. J., Diskin, G. S., Sachse, G. W., Fuelberg, H., Sessions, W. R., Harrigan, D. L., Huey, G., Liao, J., Case-Hanks,
456   A., Jimenez, J. L., Cubison, M. J., Vay, S. A., Weinheimer, A. J., Knapp, D. J., Montzka, D. D., Flocke, F. M., Pollack, I. B.,
457   Wennberg, P. O., Kurten, A., Crounse, J., Clair, J. M. S., Wisthaler, A., Mikoviny, T., Yantosca, R. M., Carouge, C. C., and Le
458   Sager, P.: Nitrogen oxides and PAN in plumes from boreal fires during ARCTAS-B and their impact on ozone: an integrated
459   analysis of aircraft and satellite observations, Atmos. Chem. Phys., 10, 9739-9760, 10.5194/acp-10-9739-2010, 2010.
460 Atkinson, R., and Arey, J.: Atmospheric Degradation of Volatile Organic Compounds, Chemical Reviews, 103, 4605-4638,
461   10.1021/cr0206420, 2003.

462 Benedict, K. B., Carrico, C. M., Kreidenweis, S. M., Schichtel, B., Malm, W. C., and Collett, J. L.: A seasonal nitrogen deposition budget
463   for Rocky Mountain National Park, Ecological Applications, 23, 1156-1169, 2013.
464 Brey, S. J., and Fischer, E. V.: Smoke in the City: How Often and Where Does Smoke Impact Summertime Ozone in the United States?,
465   Environmental Science & Technology, 50, 1288-1294, 10.1021/acs.est.5b05218, 2016.
466 Camalier, L., Cox, W., and Dolwick, P.: The effects of meteorology on ozone in urban areas and their use in assessing ozone trends,
467   Atmospheric Environment, 41, 7127-7137, http://dx.doi.org/10.1016/j.atmosenv.2007.04.061, 2007.
468 Coniglio, M. C., Correia, J., Marsh, P. T., and Kong, F.: Verification of Convection-Allowing WRF Model Forecasts of the Planetary
469   Boundary Layer Using Sounding Observations, Weather and Forecasting, 28, 842-862, 10.1175/WAF-D-12-00103.1, 2013.
470 Creamean, J. M., Neiman, P. J., Coleman, T., Senff, C. J., Kirgis, G., Alvarez, R. J., and Yamamoto, A.: Colorado air quality impacted by
471   long-range-transported aerosol: a set of case studies during the 2015 Pacific Northwest fires, Atmos. Chem. Phys., 16, 12329-
472   12345, 10.5194/acp-16-12329-2016, 2016.
473 Crosson, E. R.: A cavity ring-down analyzer for measuring atmospheric levels of methane, carbon dioxide, and water vapor, Applied
474   Physics B, 92, 403-408, 10.1007/s00340-008-3135-y, 2008.
475 Elliott, C., Henderson, S., and Wan, V.: Time series analysis of fine particulate matter and asthma reliever dispensations in populations
476   affected by forest fires, Environmental Health, 12, 11, 2013.
477 Fent, K. W., Eisenberg, J., Snawder, J., Sammons, D., Pleil, J. D., Stiegel, M. A., Mueller, C., Horn, G. P., and Dalton, J.: Systemic
478   Exposure to PAHs and Benzene in Firefighters Suppressing Controlled Structure Fires, Annals of Occupational Hygiene,
479   10.1093/annhyg/meu036, 2014.
480 Flocke, F. M., Weinheimer, A. J., Swanson, A. L., Roberts, J. M., Schmitt, R., and Shertz, S.: On the Measurement of PANs by Gas
481   Chromatography and Electron Capture Detection, Journal of Atmospheric Chemistry, 52, 19-43, 10.1007/s10874-005-6772-0,
482   2005.
483 Giglio, L., Descloitres, J., Justice, C. O., and Kaufman, Y. J.: An Enhanced Contextual Fire Detection Algorithm for MODIS, Remote
484   Sensing of Environment, 87, 273-282, http://dx.doi.org/10.1016/S0034-4257(03)00184-6, 2003.
485 Giglio, L., Csiszar, I., and Justice, C. O.: Global distribution and seasonality of active fires as observed with the Terra and Aqua Moderate
486   Resolution Imaging Spectroradiometer (MODIS) sensors, Journal of Geophysical Research: Biogeosciences, 111, n/a-n/a,
487   10.1029/2005JG000142, 2006.
488 Gilman, J. B., Lerner, B. M., Kuster, W. C., and de Gouw, J. A.: Source signature of volatile organic compounds from oil and natural gas
489   operations in northeastern Colorado, Environ Sci Technol, 47, 1297-1305, 10.1021/es304119a, 2013.
490 Gilman, J. B., Lerner, B. M., Kuster, W. C., Goldan, P. D., Warneke, C., Veres, P. R., Roberts, J. M., de Gouw, J. A., Burling, I. R., and
491   Yokelson, R. J.: Biomass burning emissions and potential air quality impacts of volatile organic compounds and other trace
492   gases from fuels common in the US, Atmos. Chem. Phys., 15, 13915-13938, 10.5194/acp-15-13915-2015, 2015.
493 Giordano, M. R., Chong, J., Weise, D. R., and Asa-Awuku, A. A.: Does chronic nitrogen deposition during biomass growth affect
494   atmospheric emissions from biomass burning?, Environmental Research Letters, 11, 034007, 2016.
495 Goode, J. G., Yokelson, R. J., Ward, D. E., Susott, R. A., Babbitt, R. E., Davies, M. A., and Hao, W. M.: Measurements of excess O3,
496   CO2, CO, CH4, C2H4, C2H2, HCN, NO, NH3, HCOOH, CH3COOH, HCHO, and CH3OH in 1997 Alaskan biomass burning
497   plumes by airborne Fourier transform infrared spectroscopy (AFTIR), Journal of Geophysical Research: Atmospheres, 105,
498   22147-22166, 10.1029/2000JD900287, 2000.
499 Guenther, A., Karl, T., Harley, P., Wiedinmyer, C., Palmer, P. I., and Geron, C.: Estimates of global terrestrial isoprene emissions using
500   MEGAN (Model of Emissions of Gases and Aerosols from Nature), Atmos. Chem. Phys., 6, 3181-3210, 10.5194/acp-6-3181-
501   2006, 2006.
502 Hobbs, P. V., Sinha, P., Yokelson, R. J., Christian, T. J., Blake, D. R., Gao, S., Kirchstetter, T. W., Novakov, T., and Pilewskie, P.:
503   Evolution of gases and particles from a savanna fire in South Africa, Journal of Geophysical Research: Atmospheres, 108, n/a-
504   n/a, 10.1029/2002JD002352, 2003.
505 Jacob, D. J., Logan, J. A., Yevich, R. M., Gardner, G. M., Spivakovsky, C. M., Wofsy, S. C., Munger, J. W., Sillman, S., Prather, M. J.,
506   Rodgers, M. O., Westberg, H., and Zimmerman, P. R.: Simulation of summertime ozone over North America, Journal of
507   Geophysical Research: Atmospheres, 98, 14797-14816, 10.1029/93JD01223, 1993.
508 Jaegle, L., Steinberger, L., Martin, R. V., and Chance, K.: Global partitioning of NOx sources using satellite observations: Relative roles
509   of fossil fuel combustion, biomass burning and soil emissions, Faraday Discussions, 130, 407-423, 10.1039/B502128F, 2005.
510 Jaffe, D. A., Chand, D., Hafner, W., Westerling, A., and Spracklen, D.: Influence of fires on O-3 concentrations in the western US,
511   Environmental Science & Technology, 42, 5885-5891, 10.1021/es800084k, 2008.
512 Jaffe, D. A., and Wigder, N. L.: Ozone production from wildfires: A critical review, Atmospheric Environment, 51, 1-10,
513   http://dx.doi.org/10.1016/j.atmosenv.2011.11.063, 2012.
514 Kalnay, E., Kanamitsu, M., Kistler, R., Collins, W., Deaven, D., Gandin, L., Iredell, M., Saha, S., White, G., Woollen, J., Zhu, Y.,
515   Leetmaa, A., Reynolds, R., Chelliah, M., Ebisuzaki, W., Higgins, W., Janowiak, J., Mo, K. C., Ropelewski, C., Wang, J., Jenne,
516   R., and Joseph, D.: The NCEP/NCAR 40-Year Reanalysis Project, Bulletin of the American Meteorological Society, 77, 437-
517   471, 10.1175/1520-0477(1996)077<0437:TNYRP>2.0.CO;2, 1996.

Atmospheric
Chemistry
and Physics
Discussions

518 Kelly, T. J., Stedman, D. H., and Kok, G. L.: Measurements of H2O2 and HNO3in rural air, Geophysical Research Letters, 6, 375-378,
519   10.1029/GL006i005p00375, 1979.
520 Kley, D., and McFarland, M.: Chemiluminescence detector for NO and NO2, Journal of Atmospheric Technology, 12, 62-69, 1980.
521 Künzli, N., Avol, E., Wu, J., Gauderman, W. J., Rappaport, E., Millstein, J., Bennion, J., McConnell, R., Gilliland, F. D., Berhane, K.,
522   Lurmann, F., Winer, A., and Peters, J. M.: Health Effects of the 2003 Southern California Wildfires on Children, American
523   Journal of Respiratory and Critical Care Medicine, 174, 1221-1228, 10.1164/rccm.200604-519OC, 2006.
524 Lacaux, J. P., Delmas, R., Jambert, C., and Kuhlbusch, T. A. J.: NO x emissions from African savanna fires, Journal of Geophysical
525   Research: Atmospheres, 101, 23585-23595, 10.1029/96JD01624, 1996.
526 Liu, X., Zhang, Y., Huey, L. G., Yokelson, R. J., Wang, Y., Jimenez, J. L., Campuzano-Jost, P., Beyersdorf, A. J., Blake, D. R., Choi, Y.,
527   St. Clair, J. M., Crounse, J. D., Day, D. A., Diskin, G. S., Fried, A., Hall, S. R., Hanisco, T. F., King, L. E., Meinardi, S.,
528   Mikoviny, T., Palm, B. B., Peischl, J., Perring, A. E., Pollack, I. B., Ryerson, T. B., Sachse, G., Schwarz, J. P., Simpson, I. J.,
529   Tanner, D. J., Thornhill, K. L., Ullmann, K., Weber, R. J., Wennberg, P. O., Wisthaler, A., Wolfe, G. M., and Ziemba, L. D.:
530   Agricultural fires in the southeastern U.S. during SEAC4RS: Emissions of trace gases and particles and evolution of ozone,
531   reactive nitrogen, and organic aerosol, Journal of Geophysical Research: Atmospheres, n/a-n/a, 10.1002/2016JD025040, 2016.
532 Lu, X., Zhang, L., Yue, X., Zhang, J., Jaffe, D. A., Stohl, A., Zhao, Y., and Shao, J.: Wildfire influences on the variability and trend of
533   summer surface ozone in the mountainous western United States, Atmos. Chem. Phys., 16, 14687-14702, 10.5194/acp-16-
534   14687-2016, 2016.
535 Mason, S. A., Field, R. J., Yokelson, R. J., Kochivar, M. A., Tinsley, M. R., Ward, D. E., and Hao, W. M.: Complex effects arising in
536   smoke plume simulations due to inclusion of direct emissions of oxygenated organic species from biomass combustion, Journal
537   of Geophysical Research: Atmospheres, 106, 12527-12539, 10.1029/2001JD900003, 2001.
538 McClure-Begley, A., Petropavlovskikh, I., and Oltmans, S.: NOAA Global Monitoring Surface Ozone Network. BAO, June 2015 -
539   September 2015. National Oceanic and Atmospheric Administration, Earth Systems Research Laboratory Global Monitoring
540   Division. Boulder, CO., doi:10.7289/V5P8WBF, 2014.
541 McDuffie, E. E., Edwards, P. M., Gilman, J. B., Lerner, B. M., Dubé, W. P., Trainer, M., Wolfe, D. E., Angevine, W. M., deGouw, J.,
542   Williams, E. J., Tevlin, A. G., Murphy, J. G., Fischer, E. V., McKeen, S., Ryerson, T. B., Peischl, J., Holloway, J. S., Aikin, K.,
543   Langford, A. O., Senff, C. J., Alvarez, R. J., Hall, S. R., Ullmann, K., Lantz, K. O., and Brown, S. S.: Influence of oil and gas
544   emissions on summertime ozone in the Colorado Northern Front Range, Journal of Geophysical Research: Atmospheres, 121,
545   8712-8729, 10.1002/2016JD025265, 2016.
546 McManus, J. B., Zahniser, M. S., and Nelson, D. D.: Dual quantum cascade laser trace gas instrument with astigmatic Herriott cell at high
547   pass number, Appl. Opt., 50, A74-A85, 10.1364/AO.50.000A74, 2011.
548 McMeeking, G. R., Kreidenweis, S. M., Baker, S., Carrico, C. M., Chow, J. C., Collett, J. L., Hao, W. M., Holden, A. S., Kirchstetter, T.
549   W., Malm, W. C., Moosmüller, H., Sullivan, A. P., and Wold, C. E.: Emissions of trace gases and aerosols during the open
550   combustion of biomass in the laboratory, Journal of Geophysical Research: Atmospheres, 114, n/a-n/a, 10.1029/2009JD011836,
551   2009.
552 Mesinger, F., DiMego, G., Kalnay, E., Mitchell, K., Shafran, P. C., Ebisuzaki, W., Jović, D., Woollen, J., Rogers, E., Berbery, E. H., Ek,
553   M. B., Fan, Y., Grumbine, R., Higgins, W., Li, H., Lin, Y., Manikin, G., Parrish, D., and Shi, W.: North American Regional
554   Reanalysis, Bulletin of the American Meteorological Society, 87, 343-360, 10.1175/bams-87-3-343, 2006.
555 Moody, J. L., Munger, J. W., Goldstein, A. H., Jacob, D. J., and Wofsy, S. C.: Harvard Forest regional-scale air mass composition by
556   Patterns in Atmospheric Transport History (PATH), Journal of Geophysical Research: Atmospheres, 103, 13181-13194,
557   10.1029/98JD00526, 1998.
558 Morris, G. A., Hersey, S., Thompson, A. M., Pawson, S., Nielsen, J. E., Colarco, P. R., McMillan, W. W., Stohl, A., Turquety, S., Warner,
559   J., Johnson, B. J., Kucsera, T. L., Larko, D. E., Oltmans, S. J., and Witte, J. C.: Alaskan and Canadian forest fires exacerbate
560   ozone pollution over Houston, Texas, on 19 and 20 July 2004, Journal of Geophysical Research: Atmospheres, 111, n/a-n/a,
561   10.1029/2006JD007090, 2006.
562 Pétron, G., Frost, G., Miller, B. R., Hirsch, A. I., Montzka, S. A., Karion, A., Trainer, M., Sweeney, C., Andrews, A. E., Miller, L., Kofler,
563   J., Bar-Ilan, A., Dlugokencky, E. J., Patrick, L., Moore, C. T., Ryerson, T. B., Siso, C., Kolodzey, W., Lang, P. M., Conway, T.,
564   Novelli, P., Masarie, K., Hall, B., Guenther, D., Kitzis, D., Miller, J., Welsh, D., Wolfe, D., Neff, W., and Tans, P.: Hydrocarbon
565   emissions characterization in the Colorado Front Range: A pilot study, Journal of Geophysical Research: Atmospheres, 117, n/a-
566   n/a, 10.1029/2011JD016360, 2012.
567 Pétron, G., Karion, A., Sweeney, C., Miller, B. R., Montzka, S. A., Frost, G. J., Trainer, M., Tans, P., Andrews, A., Kofler, J., Helmig, D.,
568   Guenther, D., Dlugokencky, E., Lang, P., Newberger, T., Wolter, S., Hall, B., Novelli, P., Brewer, A., Conley, S., Hardesty, M.,
569   Banta, R., White, A., Noone, D., Wolfe, D., and Schnell, R.: A new look at methane and nonmethane hydrocarbon emissions
570   from oil and natural gas operations in the Colorado Denver-Julesburg Basin, Journal of Geophysical Research: Atmospheres,
571   119, 6836-6852, 10.1002/2013JD021272, 2014.
572 Pfister, G. G., Wiedinmyer, C., and Emmons, L. K.: Impacts of the fall 2007 California wildfires on surface ozone: Integrating local
573   observations with global model simulations, Geophysical Research Letters, 35, n/a-n/a, 10.1029/2008GL034747, 2008.

16

Atmospheric
Chemistry
and Physics
Discussions

574 Pinder, R. W., Gilliland, A. B., and Dennis, R. L.: Environmental impact of atmospheric NH3 emissions under present and future
575   conditions in the eastern United States, Geophysical Research Letters, 35, n/a-n/a, 10.1029/2008GL033732, 2008.
576 Rappold, A. G., Stone, S. L., Cascio, W. E., Neas, L. M., Kiларu, V. J., Carraway, M. S., Szykman, J. J., Ising, A., Cleve, W. E., Meredith,
577   J. T., Vaughan-Batten, H., Deyneka, L., and Devlin, R. B.: Peat Bog Wildfire Smoke Exposure in Rural North Carolina Is
578   Associated with Cardiopulmonary Emergency Department Visits Assessed through Syndromic Surveillance, Environmental
579   Health Perspectives, 119, 1415-1420, 10.1289/ehp.1003206, 2011.
580 Reddy, P. J., and Pfister, G. G.: Meteorological factors contributing to the interannual variability of midsummer surface ozone in Colorado,
581   Utah, and other western U.S. states, Journal of Geophysical Research: Atmospheres, 121, 2434-2456, 10.1002/2015JD023840,
582   2016.
583 Roberts, J. M., Flocke, F., Chen, G., de Gouw, J., Holloway, J. S., Hübler, G., Neuman, J. A., Nicks, D. K., Nowak, J. B., Parrish, D. D.,
584   Ryerson, T. B., Sueper, D. T., Warneke, C., and Fehsenfeld, F. C.: Measurement of peroxycarboxylic nitric anhydrides (PANs)
585   during the ITCT 2K2 aircraft intensive experiment, Journal of Geophysical Research: Atmospheres, 109, n/a-n/a,
586   10.1029/2004JD004960, 2004.
587 Rolph, G. D., Draxler, R. R., Stein, A. F., Taylor, A., Ruminski, M. G., Kondragunta, S., Zeng, J., Huang, H.-C., Manikin, G., McQueen, J.
588   T., and Davidson, P. M.: Description and Verification of the NOAA Smoke Forecasting System: The 2007 Fire Season, Weather
589   and Forecasting, 24, 361-378, 10.1175/2008WAF2222165.1, 2009.
590 Roscioli, J. R., Zahniser, M. S., Nelson, D. D., Herndon, S. C., and Kolb, C. E.: New Approaches to Measuring Sticky Molecules:
591   Improvement of Instrumental Response Times Using Active Passivation, The Journal of Physical Chemistry A, 120, 1347-1357,
592   10.1021/acs.jpca.5b04395, 2016.
593 Rudolph, J., and Ehhalt, D. H.: Measurements of C2–C5 hydrocarbons over the North Atlantic, Journal of Geophysical Research: Oceans,
594   86, 11959-11964, 10.1029/JC086iC12p11959, 1981.
595 Schreier, S. F., Richter, A., Schepaschenko, D., Shvidenko, A., Hilboll, A., and Burrows, J. P.: Differences in satellite-derived NOx
596   emission factors between Eurasian and North American boreal forest fires, Atmospheric Environment, 121, 55-65,
597   http://dx.doi.org/10.1016/j.atmosenv.2014.08.071, 2015.
598 Sillman, S.: The relation between ozone, NOx, and hydrocarbons in urban and polluted rural environments, Atmospheric Environment, 33,
599   1821-1845, 1999.
600 Singh, H. B., Cai, C., Kaduwela, A., Weinheimer, A., and Wisthaler, A.: Interactions of fire emissions and urban pollution over California:
601   Ozone formation and air quality simulations, Atmospheric Environment, 56, 45-51, 10.1016/j.atmosenv.2012.03.046, 2012.
602 Sive, B. C., Zhou, Y., Troop, D., Wang, Y., Little, W. C., Wingenter, O. W., Russo, R. S., Varner, R. K., and Talbot, R.: Development of a
603   Cryogen-Free Concentration System for Measurements of Volatile Organic Compounds, Analytical Chemistry, 77, 6989-6998,
604   10.1021/ac0506231, 2005.
605 Stein, A. F., Draxler, R. R., Rolph, G. D., Stunder, B. J. B., Cohen, M. D., and Ngan, F.: NOAA's HYSPLIT Atmospheric Transport and
606   Dispersion Modeling System, Bulletin of the American Meteorological Society, 96, 2059-2077, 10.1175/BAMS-D-14-00110.1,
607   2015.
608 Stockwell, C. E., Veres, P. R., Williams, J., and Yokelson, R. J.: Characterization of biomass burning emissions from cooking fires, peat,
609   crop residue, and other fuels with high-resolution proton-transfer-reaction time-of-flight mass spectrometry, Atmos. Chem. Phys.,
610   15, 845-865, 10.5194/acp-15-845-2015, 2015.
611 Swarthout, R. F., Russo, R. S., Zhou, Y., Hart, A. H., and Sive, B. C.: Volatile organic compound distributions during the NACHTT
612   campaign at the Boulder Atmospheric Observatory: Influence of urban and natural gas sources, Journal of Geophysical
613   Research: Atmospheres, 118, 10,614-610,637, 10.1002/jgrd.50722, 2013.
614 Tabazadeh, A., Jacobson, M. Z., Singh, H. B., Toon, O. B., Lin, J. S., Chatfield, R. B., Thakur, A. N., Talbot, R. W., and Dibb, J. E.: Nitric
615   acid scavenging by mineral and biomass burning aerosols, Geophysical Research Letters, 25, 4185-4188,
616   10.1029/1998GL900062, 1998.
617 Thompson, C. R., Hueber, J., and Helmig, D.: Influence of oil and gas emissions on ambient atmospheric non-methane hydrocarbons in
618   residential areas of Northeastern Colorado, Elementa: Science of the Anthropocene, 2, 000035,
619   10.12952/journal.elementa.000035, 2014.
620 Townsend-Small, A., Botner, E. C., Jimenez, K. L., Schroeder, J. R., Blake, N. J., Meinardi, S., Blake, D. R., Sive, B. C., Bon, D.,
621   Crawford, J. H., Pfister, G., and Flocke, F. M.: Using stable isotopes of hydrogen to quantify biogenic and thermogenic
622   atmospheric methane sources: A case study from the Colorado Front Range, Geophysical Research Letters, 43, 11,462-411,471,
623   10.1002/2016GL071438, 2016.
624 Trentmann, J., Yokelson, R. J., Hobbs, P. V., Winterrath, T., Christian, T. J., Andreae, M. O., and Mason, S. A.: An analysis of the
625   chemical processes in the smoke plume from a savanna fire, Journal of Geophysical Research: Atmospheres, 110, n/a-n/a,
626   10.1029/2004JD005628, 2005.
627 Val Martin, M., Heald, C. L., Lamarque, J. F., Tilmes, S., Emmons, L. K., and Schichtel, B. A.: How emissions, climate, and land use
628   change will impact mid-century air quality over the United States: a focus on effects at national parks, Atmos. Chem. Phys., 15,
629   2805-2823, 10.5194/acp-15-2805-2015, 2015.

630   Westerling, A. L.: Increasing western US forest wildfire activity: sensitivity to changes in the timing of spring, Philosophical Transactions
631   of the Royal Society B: Biological Sciences, 371, 2016.
632   Yates, E. L., Iraci, L. T., Singh, H. B., Tanaka, T., Roby, M. C., Hamill, P., Clements, C. B., Lareau, N., Contezac, J., Blake, D. R.,
633   Simpson, I. J., Wisthaler, A., Mikoviny, T., Diskin, G. S., Beyersdorf, A. J., Choi, Y., Ryerson, T. B., Jimenez, J. L.,
634   Campuzano-Jost, P., Loewenstein, M., and Gore, W.: Airborne measurements and emission estimates of greenhouse gases and
635   other trace constituents from the 2013 California Yosemite Rim wildfire, Atmospheric Environment, 127, 293-302,
636   http://dx.doi.org/10.1016/j.atmosenv.2015.12.038, 2016.
637   Yokelson, R. J., Crounse, J. D., DeCarlo, P. F., Karl, T., Urbanski, S., Atlas, E., Campos, T., Shinozuka, Y., Kapustin, V., Clarke, A. D.,
638   Weinheimer, A., Knapp, D. J., Montzka, D. D., Holloway, J., Weibring, P., Flocke, F., Zheng, W., Toohey, D., Wennberg, P. O.,
639   Wiedinmyer, C., Mauldin, L., Fried, A., Richter, D., Walega, J., Jimenez, J. L., Adachi, K., Buseck, P. R., Hall, S. R., and
640   Shetter, R.: Emissions from biomass burning in the Yucatan, Atmos. Chem. Phys., 9, 5785-5812, 10.5194/acp-9-5785-2009,
641   2009.
642   Zaragoza, J.: Observations of acyl peroxy nitrates during the Front Range Air Pollution And Photochemistry Éxperiment (FRAPPÉ),
643   Master of Science (M.S.), Atmospheric Science, Colorado State University, 78 pp., 2016.
644
645

646
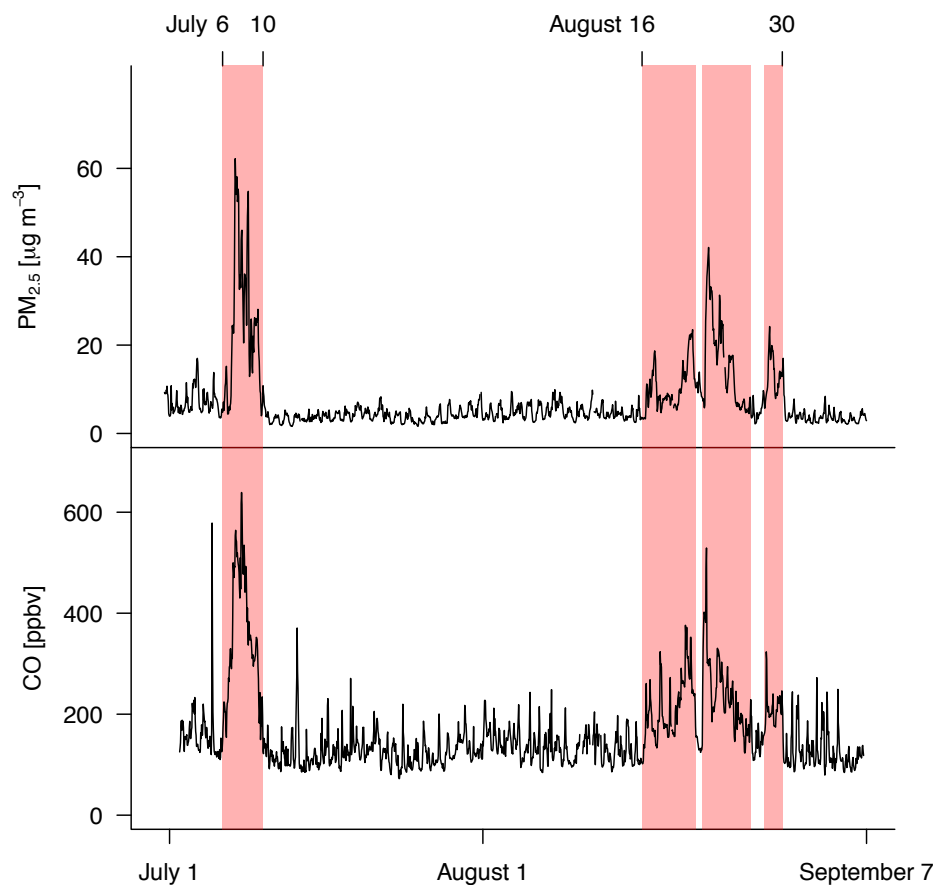
Figure 1. Top panel: Time series of hourly PM$_{2.5}$ concentrations for the CDPHE CAMP air quality monitoring site (www.epa.gov/airdata) located in downtown Denver (39.75', -104.98'). Bottom panel: Time series of hourly CO mixing ratios at the Boulder Atmospheric Observatory (BAO: 40.05', -105.01'). Red shading denotes periods during which smoke is present at BAO.

650

651

Atmospheric
Chemistry
and Physics
Discussions
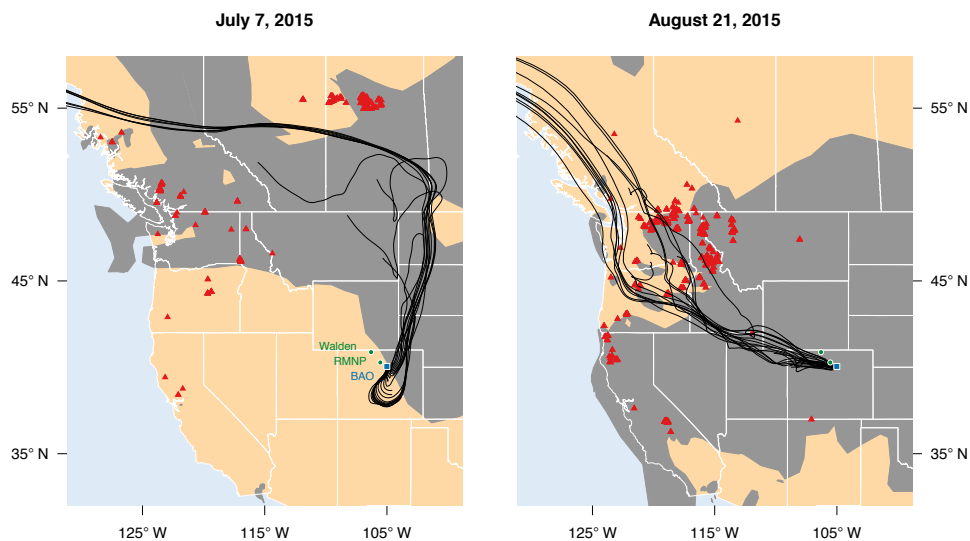
Figure 2. Representative days during each smoke period observed at the Boulder Atmospheric Observatory (BAO: blue square). NOAA Hazard Mapping System (http://www.ssd.noaa.gov/PS/FIRE/) smoke polygons are plotted in grey with MODIS fire locations (http://modis-fire.umd.edu/index.php) from the previous day plotted as red triangles. The thin black lines show HYSPLIT back trajectories from the BAO site initiated 1000 m a.g.l. for each hour of the day plotted.

Atmospheric
Chemistry
and Physics
Discussions

657
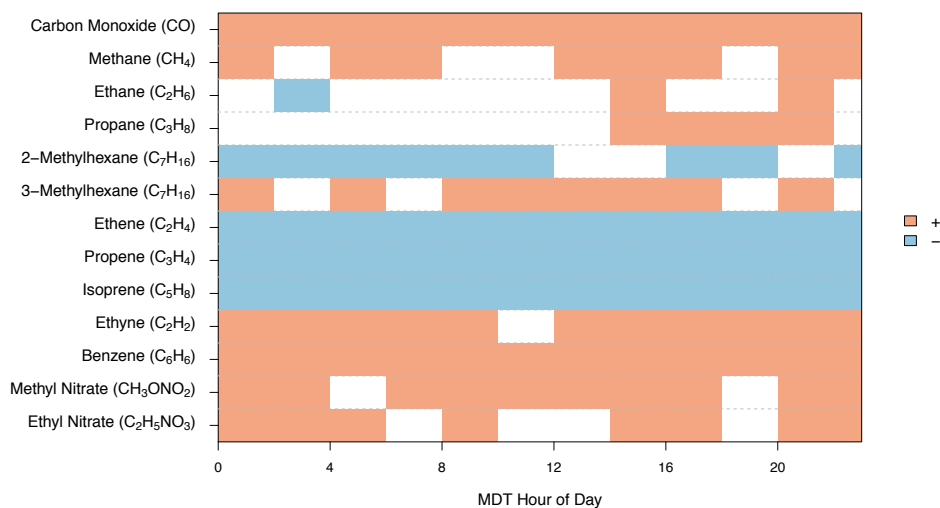
Figure 3. Significant changes (two sided Student's t-test, 90% confidence interval) in hourly averaged mixing ratios of a subset of
species measured at BAO between smoke-free periods and the 16 - 30 August smoke period. Significant increases during smoke-
**impacted periods compared to smoke-free periods are shown in red, significant decreases are in blue.**

661
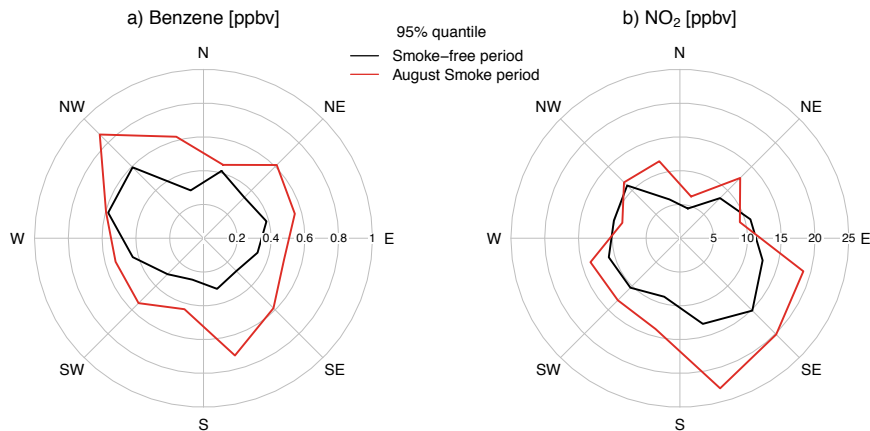
Figure 4. 95th percentiles of a) benzene and b) NO_2 as a function of wind direction for all data during smoke-free periods (black)
**and the August smoke period (red).**

664
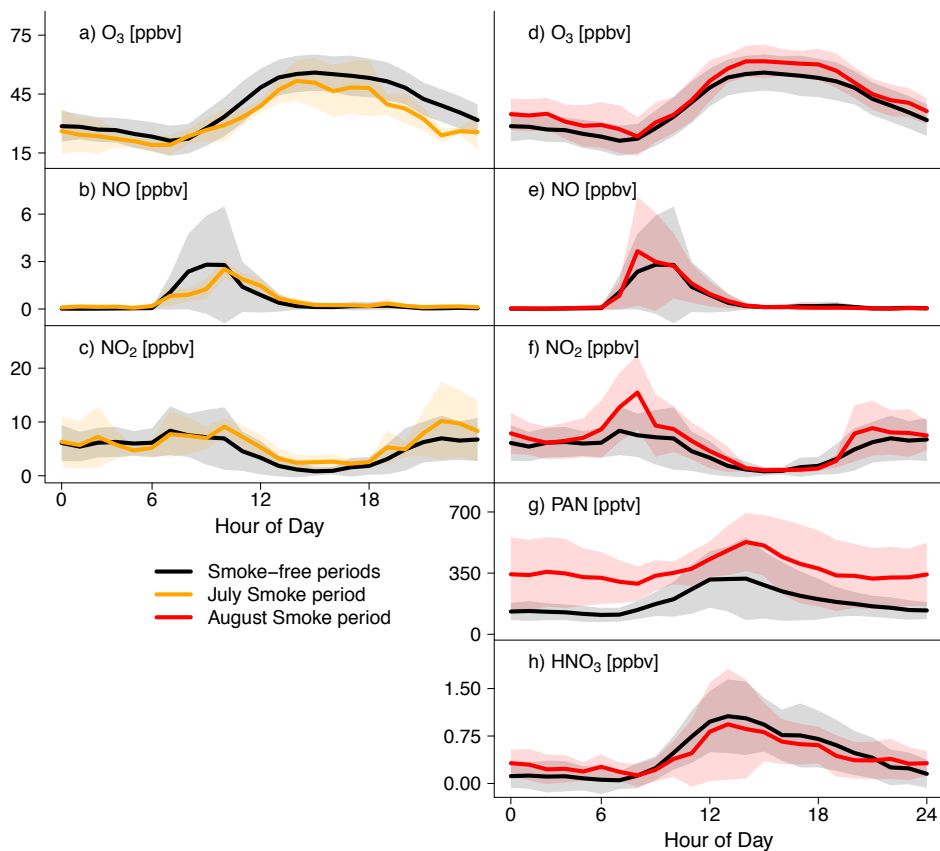
Figure 5. Average diurnal cycles in MDT of O_3 and oxidized reactive nitrogen species at BAO. Panels a), b), and c) compare average diurnal cycles from smoke-free time periods (black) to average diurnal cycles from the July smoke-impacted period (orange). Panels d) – h) show average diurnal cycles during the August smoke-impacted period (red) to the same average diurnal cycles from smoke-free periods (black). PAN and HNO_3 measurements were not available during the July smoke-impacted period.

669
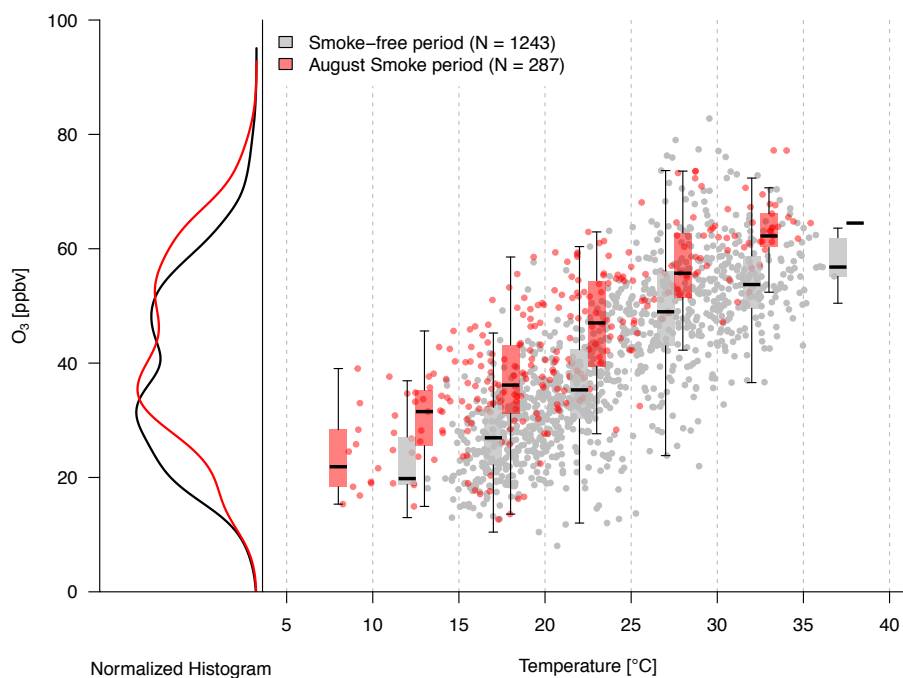
Figure 6. Hourly O$_3$ data from BAO plotted against hourly temperature data show a positive correlation between temperature and O$_3$ abundances for both smoke-free time periods in grey and the August smoke-impacted time period in red. Overlaid are boxplots (5th, 25th, 50th, 75th, and 95th percentiles) for each 5 °C bin. On the left normalized histograms of the hourly O$_3$ data are plotted, with all smoke-free measurements in black, and all hourly measurements made during the August smoke-impacted period in red.

Atmospheric
Chemistry
and Physics
Discussions

674
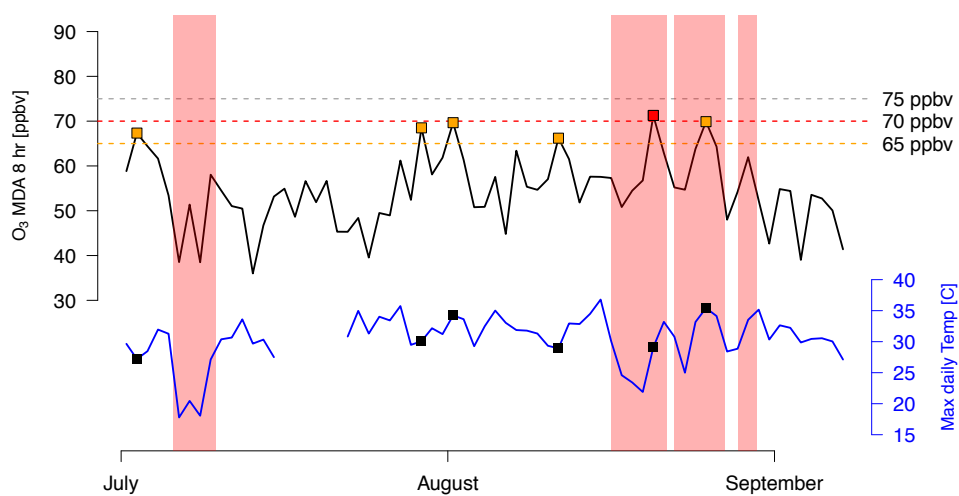
Figure 7. Maximum daily 8-hour average (MDA8) O$_3$ mixing ratios at BAO plotted in black with maximum daily temperature at
BAO in blue. Orange and red boxes denote days that exceed 65 and 70 ppbv respectively.

Atmospheric
Chemistry
and Physics
Discussions

Open Access

EGU

677
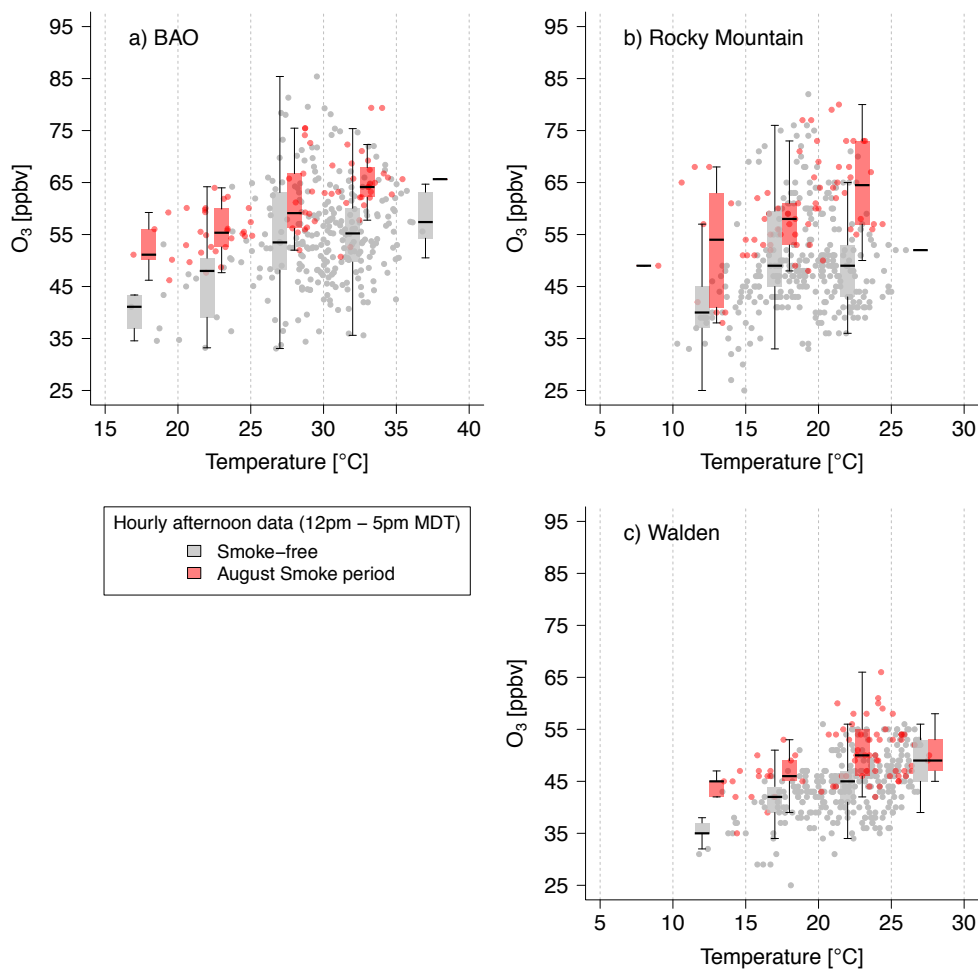
Figure 8. Hourly O$_3$ versus temperature for a) BAO, b) the Rocky Mountain National Park long-term monitoring site, and c) the Arapahoe National Wildlife Refuge long-term monitoring site near Walden, CO. Plotted here are hourly afternoon data (12PM – 5PM MDT), with boxplots showing standard percentiles of 5 °C binned O$_3$ data the same as was shown in Figure 6.

25